An Extreme Value Mixture model to assess drought hazard in West Africa

Abdoulaye Sy, Catherine Araujo-Bonjean, Marie-Eliette Dury, Nourddine Azzaoui, Arnaud Guillin

CENTRE D'ÉTUDES
ET DE RECHERCHES
SUR LE DEVELOPPEMENT
INTERNATIONAL

SÉRIE ÉTUDES ET DOCUMENTS

An Extreme Value Mixture model to assess drought hazard in West Africa

Abdoulaye Sy
Catherine Araujo-Bonjean
Marie-Eliette Dury
Nourddine Azzaoui
Arnaud Guillin

Études et Documents n°23
July 2021

To cite this document:

Sy A., Araujo-Bonjean C., Dury M-E., Azzaoui N., Guillin A. (2021) "An Extreme Value Mixture model to assess drought hazard in West Africa", *Études et Documents,* n°23, CERDI.

CERDI
POLE TERTIAIRE
26 AVENUE LÉON BLUM
F- 63000 CLERMONT FERRAND
TEL. + 33 4 73 17 74 00
FAX + 33 4 73 17 74 28
http://cerdi.uca.fr/

The authors

Abdoulaye Sy
Postdoctoral researcher, Université Clermont Auvergne, CNRS, IRD, CERDI, F-63000 Clermont-Ferrand, France
Email address: abdoulaye.sy@uca.fr

Catherine Araujo-Bonjean
CNRS Researcher, Université Clermont Auvergne, CNRS, IRD, CERDI, F-63000 Clermont-Ferrand, France
Email address: catherine.araujo-bonjean@uca.fr

Marie-Eliette Dury
Associate professor, Université Clermont Auvergne, CNRS, IRD, CERDI, F-63000 Clermont-Ferrand, France
Email address: m-eliette.dury@uca.fr

Nourddine Azzaoui
Associate professor, Université Clermont Auvergne, CNRS, LMBP, F-63000 Clermont-Ferrand, France
Email address: nourddine.azzaoui@uca.fr

Arnaud Guillin
Professor, Université Clermont Auvergne, CNRS, LMBP, F-63000 Clermont-Ferrand, France
Email address: arnaud.guillin@uca.fr

Corresponding author: Abdoulaye Sy

This work was supported by the LABEX IDGM+ (ANR-10-LABX-14-01) within the program "Investissements d'Avenir" operated by the French National Research Agency (ANR).

Études et Documents are available online at: https://cerdi.uca.fr/etudes-et-documents/

Director of Publication: Grégoire Rota-Graziosi
Editor: Catherine Araujo-Bonjean
Publisher: Aurélie Goumy
ISSN: 2114 - 7957

Disclaimer:

Études et Documents is a working papers series. Working Papers are not refereed, they constitute research in progress. Responsibility for the contents and opinions expressed in the working papers rests solely with the authors. Comments and suggestions are welcome and should be addressed to the authors.

Abstract

A critical stage in drought hazard assessment is the definition of a drought event, and the measure of its intensity. Actually, the classical approach imposes to all climatic region the same set of thresholds for drought severity classification, hence resulting in a loss of information on rare events in the distribution tails, which are precisely the most important to catch in risk analysis. In order to better assess extreme events, we resort to an extreme value mixture model with a normal distribution for the bulk and a Generalized Pareto distribution for the upper and lower tails, to estimate the intensity of extreme droughts and their occurrence probability. Compare to the standard approach to drought hazard, which relies on a standardized precipitation index and a classification of drought intensity established from the cumulative standard normal distribution function, our approach allows the drought threshold and the occurrence probability of drought to depend on the specific characteristics of each precipitation distribution. An application to the West Africa region shows that the accuracy of our mixture model is higher than that of the standard model. The mixture performs better at modelling the lowest percentiles and specifically the return level of the centennial drought, which is generally overestimated in the standard approach.

Keywords

Mixture model, Generalized pareto distribution, Drought hazard, Extreme value theory

JEL Codes

C15, Q54

Acknowledgment

The authors acknowledge the support received from the Agence Nationale de la Recherche of the French government though the IDEX-ISITE initiative (16-IDEX-0001 CAP 20-25) and the LABEX IDGM+ (ANR-10-LABX-14-01), within the program ‘‘Investissements d’Avenir’’.

1. Introduction

This study takes place in the strand of literature dedicated to drought risk assessment (e.g. Carrao et al 2016). In sub-Saharan Africa, drought is a major and recurrent threat for people, economic activity and environment. Rainfed agriculture is the dominant production system so that the agricultural sector, which contributes for a large part to the gross domestic product, is directly exposed to dry spells. In these low-income countries, droughts have long-lasting effects that can be felt long after weather conditions have returned to normal. Human and physical capital losses caused by drought often result in protracted food crisis, and contribute to poverty trap. Drought events have also spillover effects on regions or countries that are not directly affected by the hazard but are connected by trade. Food price spikes resulting from production shortfalls tend to propagate to trading partners that import or export the food products. Therefore, in sub-Saharan Africa, severe droughts are associated to food insecurity, even famine and human loss, conflicts and economic slowdown (O'Grada 2007). This was the case in the beginning of the 70s and 80s, and more recently in 2010-2011, three periods of extreme drought that have marked the continent's history.

Despite the pervasive impact of droughts in Africa, drought risk management strategies have long been limited to ex-post emergency responses (Wilhite et al 2014). This situation led the United Nations Convention to Combat Desertification to plaid for urgent actions at the global, regional and national level, to establish a strategic framework for drought risk management in Africa (UNCCD, WMO and FAO 2018). To define a consistent framework for drought risk management, and enhance resilience to drought, one prerequisite is to identify and understand the drought risk components (Hayes et al. 2004).

The risk associated with a natural hazard is defined as the potential loss from the hazard. It is commonly view as the combination of three components: hazard, exposure and vulnerability (Dilley et al 2005; IPCC 2012). Therefore, depending on the vulnerability of exposed socioeconomic and natural systems, a natural hazard may become a disaster.

Hazard, the first component of risk, can be defined as the probability of occurrence of a potentially damaging event (Rajsekhar et al 2015). The difficulty in measuring drought hazard comes from the multiplicity of drought definitions. There is no unique definition of drought, and drought assessment is necessarily region and impact specific (Wilhite and Glantz 1985). As other natural hazards, droughts can be characterized in terms of their severity, location, duration and timing (WMO and GWP 2016). But droughts differ from other natural hazards in many respects. Droughts are slow-onset, large-scale and long-duration phenomena. They result from large-scale anomalies in atmospheric circulation, require a minimum of two to three months to become established, and persist for months, seasons or years. Therefore, the onset and end of droughts, their intensity and spatial characteristics are difficult to assess.

Drought is also a socioeconomic construct, which definition relates to its impact. The climatological community has defined four types of drought: meteorological drought, agricultural drought, hydrological drought, and socioeconomic drought (Wilhite and Glantz 1985; WMO and GWP 2016). Meteorological drought is defined as a prolonged dry period in the natural climate cycle. Thus, meteorological drought is a relative, rather than absolute phenomenon, specific to a region, that can occur in any part of the world whether arid or wet

(Wilhite 2000). It is measured by departure from normal precipitations over some specified period of time. Agricultural droughts originate from soil water depletion during a specific growing stage of the crop leading to reduced yields. A commonly used index to assess agricultural droughts is the Standardized Precipitation Evapotranspiration Index (SPEI), which combines precipitation and evapotranspiration indicators to catch soil moisture (Vicente-Serrano et al. 2010). Hydrological drought refers to persistent low surface or subsurface water supply, in streams, rivers, reservoirs, or groundwater. The Palmer Drought Severity Index (Palmer 1965) is used to assess this type of long-term drought, which usually results from a prolonged meteorological drought. The index combines temperature and water balance indicators. Socioeconomic drought occurs when the demand for water exceeds the supply for domestic use or economic activity (for instance hydroelectric energy production or irrigation).

All types of drought originate from a deficiency of precipitation, i.e. a meteorological drought that propagates to other types of drought (agricultural, hydrological and socioeconomic) (Wilhite 2000). Whatever the type of drought, the intensity of drought is not evaluated upon its social or economic impact but in relation to the climatologic norm for the region or to the demand for water in the region or sector of activity. Droughts intensity being generally the main, or even the sole, criterion used to assess drought hazard, the measurement of drought intensity plays a crucial role in estimating drought risk

The reference classification system for drought severity is that of McKee et al (1993). It has been established for a standardized index, namely the Standardized Precipitation Index (SPI). The SPI measures cumulated precipitation deviations from their long-term mean. It can be computed over several intervals of time e.g. 3, 6, 12 months or more. Based on precipitations, the SPI specifically assesses the intensity of meteorological droughts but depending on the considered time scale, it can also be informative on other types of drought. The raw precipitation data are fitted to an incomplete Gamma distribution and then transformed to Gaussian equivalents with zero mean and variance equal to one (see for more computational details Guttman 1999; Edwards and McKee 1997). Therefore, SPI values are dimensionless, comparable across regions with different climatic regimes, and they offer a readily interpretable measure of drought intensity. McKee et al (1993) distinguished four types of droughts from mild to severe, according to the SPI values and a fixed set of threshold values.

Working with a standardized index of drought, such as the SPI, and using the classification of McKee et al (1993), the standard procedure to compute a drought hazard index (DHI) consists in giving weights to each drought category. Then the DHI is the weighted sum of the frequency of occurrence of each type of drought. Alternatively, each drought category can be further split into subcategories corresponding to different occurrence probabilities, from low to high, with increasing ratings. Thus, the DHI is calculated by combining the weights and ratings of the various subcategories of droughts. The sub-classification can be arbitrarily chosen (Shahid and Behrawan 2008) or identified using a natural break classification method (Carrao et al 2014; Rajsekhar et al 2015; He et al 2013).

The main advantage of this approach to drought classification and hazard estimation, based on a standardized index, is to offer a comprehensive and consistent framework allowing comparing precipitation depth across regions. However, the standardization process imposes a common distribution to the transformed-data and the same set of thresholds for drought

classification. Therefore, each class of drought has the same probability of occurrence and the same intensity whatever the geographical location (Carrao et al 2014). More importantly, standardization results in a loss of information on the characteristics of precipitation deficit, especially on rare events in the distribution tails, which are precisely the most important to catch in risk analysis.

In this paper, we focus on extreme events, and propose an alternative method to drought hazard estimation based on extreme value theory. Compared to previous ones, our approach does not impose a unique set of thresholds for drought classification nor standardization, or any other transformation, of the precipitation data. The drought threshold and the probability of occurrence of a drought are estimated, location by location, using an extreme value mixture model with a normal distribution for the bulk, and a Generalized Pareto distribution (GPD) for the upper and lower tails of the rainfall distribution. The great advantage of this approach is to provide estimation of droughts' intensity and of their probability of occurrence that are specific to each geographical location. As a consequence, the drought hazard index can be measured more precisely, using the estimated intensity of each drought event instead of a somehow arbitrary system of weights and rating. Another advantage of our method is to provide an estimation of the drought threshold in the same unit than the raw data, allowing setting up an operational drought monitoring system.

To test the relevance of our approach to drought hazard estimation we work on a gridded set of rainfall data covering West Africa, from January 1901 to December 2016. Although the study area is limited, it includes a wide range of climatic zones. To facilitate comparisons with the standard approach of drought classification and DHI evaluation, we focus on meteorological droughts measured from cumulated annual rainfall. For ease of interpretation most of the results are provided in the form of maps.

The remainder of the paper is organized as follows. Section 2 presents the extreme value mixture model. Section 3 describes the studied area and the database. Section 4 provides the estimation results. Section 5 compares our estimation of drought hazard with that obtained using the standard approach. Section 6 concludes.

2. The extreme value mixture model

We focus on extreme precipitation events in the lower tail of the rainfall distribution. Drawing on the extreme value theory, we define the drought threshold as the precipitation value below which precipitation distribution can be approximated by an extreme value model. Symmetrically, we consider that heavy precipitation, above an upper threshold, can also be approximated by an extreme value model.

To estimate these thresholds separating the bulk of the distribution from the tails, mixture models are of great interest. Thanks to their ability to adapt to a wide variety of random phenomena, mixture models play an important role in statistical data analysis. They have been successfully used in a myriad of applications and statistical data engineering, for instance in the fields of econometrics as well as biology and epidemiology, meteorology, and more recently Machine learning. The general idea of the model is to express the underlying distribution as a weighted sum of a given family of reference distributions. In our context, we

are interested only in finite mixture models i.e. finite weighted sums. Let us denote $X_1, \dots, X_T$ a random sample from a finite mixture of m arbitrary distributions possibly d-vector valued; the density function f of X_k can be defined, for all $x_i \in \mathbb{R}^d$, as follows:

$$f_\Theta(x_i) = \sum_{j=1}^{m} \pi_j \varphi_j(x_i), \qquad where \qquad \sum_{j=1}^{m} \pi_j = 1.$$

Denote $\Theta = (\Pi, \boldsymbol{\phi}) = (\pi_1, \dots, \pi_m, \varphi_1, \dots, \varphi_m)$ an object describing the mixture density of the sample. We assume that the densities φ_j are drawn from some family $\mathcal{F}$ of multivariate density functions. Mixtures are said to be parametric or semi-parametric when the elements of $\mathcal{F}$ are completely described by a finite or a discrete number of scalars. Gaussian mixtures are, by far, the most popular and most used parametric mixture models in literature either in Gaussian regressions or in clustering problems. In this case:

$$\mathcal{F}_g = \{\varphi(\cdot\,|\mu, \sigma^2) = \text{ density of } \mathcal{N}(\mu, \sigma^2), (\mu, \sigma^2) \in \mathbb{R} \times \mathbb{R}_+^*\}$$

where $\mathcal{N}(\mu, \sigma^2)$ is the normal distribution of mean $\mu \in \mathbb{R}$ and variance $\sigma^2 > 0$, with probability density function defined for all $x \in \mathbb{R}$ by

$$\varphi(x|\mu, \sigma^2) = \frac{1}{\sigma_k \sqrt{2\pi}} \exp\left(-\frac{1}{2}\left(\frac{x - \mu_k}{\sigma_k}\right)^2\right)$$

The general representation of the model reduces so that the parameters become $\Theta = (\Pi, \boldsymbol{\phi}) = (\pi_1, \dots, \pi_m, \mu_1, \sigma_1, \dots, \mu_m, \sigma_m)$.

Despite their success and popularity, Gaussian mixtures are not convenient to model rare and extreme events that are intrinsically linked to precipitation data. In the aim to model these events we draw on the "Peak Over Threshold" (POT) approach of Pickands (1975). Under the conditions of the Pickands-Balkema-de Haan theorem, the asymptotic distribution of observations *X* exceeding a sufficiently high threshold is a Generalized Pareto distribution (GPD). Therefore, we adopt the generalized Pareto family to model the precipitation tails:

$$\mathcal{F}_p = \{\varphi(\cdot\,|u, \sigma, \xi) = \text{ density of } GPD(u, \sigma, \xi) \text{ for } (u, \sigma, \xi) \in \mathbb{R} \times \mathbb{R}_+^* \times \mathbb{R}\}$$

where $GPD(u, \sigma, \xi)$ is the Generalized Pareto distribution with location parameter $u \in \mathbb{R}$, scale parameter $\sigma > 0$ and shape parameter $\xi \in \mathbb{R}$. For all the rest of the paper we will take parametric mixtures:

$$\mathcal{F} = \mathcal{F}_g \cup \mathcal{F}_p$$

We consider a particular mixture model, denoted GNG, with m=3: a generalized Pareto distribution for the upper and lower tails, and a normal for the bulk of the distribution.
The cumulative distribution function for the GNG mixture is given by[1]:

$$F(x) = \begin{cases} \phi_l G_l\left(x \middle| u_l, \sigma_l, \xi_l\right) & x < u_l \\ \phi_l + \left(1 - \phi_l - \phi_u\right)\left[\dfrac{H(x) - H(u_l)}{H(u_u) - H(u_l)}\right] & u_l \leq x \leq u_u \\ \left(1 - \phi_u\right) + \phi_u G_u\left(x \middle| u_u, \sigma_u, \xi_u\right) & x > u_u \end{cases}$$

[1] See Hu and Scarrott (2018).

H(*x*) is the normal cumulative distribution function, *G*(*x*) the conditional GPD cumulative distribution function. The parameters to be estimated are: the location parameters u_l and u_u, defining respectively the lower and upper tail thresholds; σ_l the lower tail GPD scale parameter; ξ_l the lower tail GPD shape parameter; σ_u the upper tail GPD scale parameter; ξ_u the upper tail GPD shape parameter. The tail fractions ϕ_u and ϕ_l represent, respectively, the probability of being above the upper threshold and the probability of being below the lower threshold. In our estimations they are given by: $\phi_l = H(u_l)$ and $\phi_u = 1 - H(u_u)$ so that *F*(*x*) reduces to:

$$\mathrm{F}(x) = \begin{cases} H(u_l)G_l(x) & x < u_l \\ H(x) & u_l \leq x \leq u_u \\ H(u_u) + \big(1 - H(u_u)\big)\ G_u(x) & x > u_u \end{cases}$$

The conditional GDP cumulative distribution function up to the lower threshold is given by:

$$G_l\big(x \big| u_l, \sigma_l, \xi_l\big) = \Pr(X < x | X < u_l) = \begin{cases} \left[1 + \xi_l\left(\frac{u_l - x}{\sigma_l}\right)\right]^{-1/\xi_l} & \text{if } \xi_l \neq 0, \\ \exp\left[-\left(\frac{u_l - x}{\sigma_l}\right)\right] & \text{if } \xi_l = 0 \end{cases}$$

for all $x \in \left]u_l + \frac{\sigma_l}{\xi_l}; u_l\right[$ if $\xi_l < 0$; for all $x < u_l$ if $\xi_l \geq 0$

The conditional GDP cumulative distribution function above the upper threshold is given by:

$$G_u\big(x \big| u, \sigma_u, \xi_u\big) = \Pr(X < x | X > u_u) = \begin{cases} 1 - \left[1 + \xi_u\left(\frac{x - u_u}{\sigma_u}\right)\right]^{-1/\xi_u}, & \text{if } \xi_u \neq 0 \\ 1 - \exp\left[-\left(\frac{x - u_u}{\sigma_u}\right)\right], & \text{if } \xi_u = 0 \end{cases}$$

for all $x \in \left]u_u; u_u - \frac{\sigma}{\xi_u}\right[$ if $\xi_u < 0$; for all $x > u_u$ if $\xi_u \geq 0$.

The shape parameter (ξ) determines the tail behavior: if $\xi = 0$, the distribution has an exponential, light tailed, distribution and belongs to the Gumbel family; if $\xi < 0$ the distribution has short bounded tail and belongs to the Weibull family; if $\xi > 0$ the distribution has a heavier tail and belongs to the Fréchet family. As an illustration, Fig. 1 depicts the density of a Gaussian law and of a mixture with two Weibull distributions for the tails, and a normal for the bulk. Figure 2 shows the sensitivity of the left threshold to the shape parameter of the GPD: the threshold is close to the mean when ξ_u is positive, and moves away from it when ξ_u is negative.

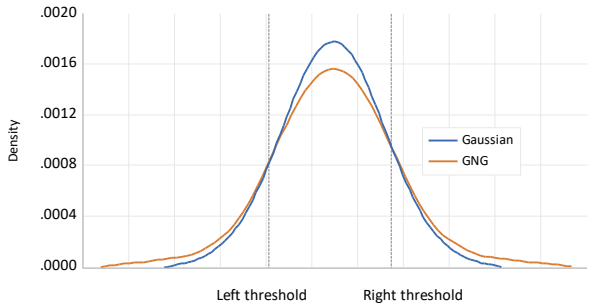

Fig. 1 Results of simulations: probability density of a GPD – Normal – GPD mixture (red) and of Gaussian distribution (blue). The two distributions have the same mean.

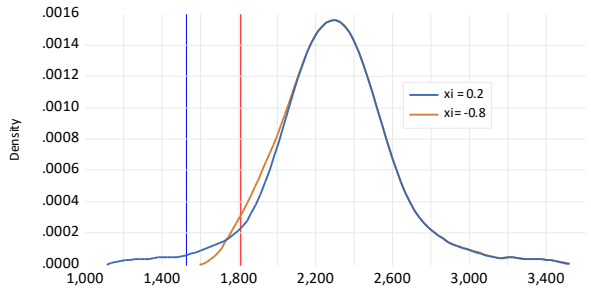

Fig. 2 Drought threshold for different values of the shape parameters of the left tail GPD (ξ_l)

Parameters estimation can be handled by numerous techniques from graphical to Bayesian methods. In what follow, we use the maximum likelihood (ML) estimator and the Evmix R package for estimations (Hu and Scarrott 2018).

3. Region and Data

The region under study is located between latitudes 0 and 18°N, and longitude 20°W and 20°E (Fig. 3). This area is centered on West Africa but includes also a part of Central Africa. Rainfall patterns in this region are determined by the monsoon system and topography. The region encompasses three major climatic areas and several climate transition zones, which cross the region from east to west, forming virtually parallel strips from the Tropic of Cancer to the Equator.

In the north of the studied area, above latitude 18°N, the climate is semi-desert, of northern Sahelian type, or desert. The rainy season is concentrated over 1 or 2 months, average annual rainfall varies from 300 mm to less than 100 mm. Further south, the tropical climate is characterized by very distinct dry and wet seasons. The length of the wet season and the amount of annual rainfall allows distinguishing 3 types of tropical climates. The Sahelian climate, or semi-arid tropical, lies between latitudes 12°N and 18°N; the dry season lasts 7 to 10 months, and the average annual rainfall varies between 300 and 700 mm. The Sudanian climate, or pure tropical, corresponds to a dry season of 5 to 6 months, with an average annual rainfall between 700 and 1000 mm (1200 mm on the Senegalese coast). The Guinean climate, or transitional tropical, corresponds to a shorter dry season, from 4 to 5 months, and an average annual rainfall above 1000 mm. The transitional equatorial and equatorial climate lie below 10°N over the countries of the Gulf of Guinea. Annual precipitations are abundant,

generally above 1000 mm with a bimodal distribution (two dry seasons). However, the rainfall distribution is quite heterogeneous in this area. The climate is very humid, with annual rainfall above 2500 mm, in the coastal regions of Guinea, Cameroon and Gabon, which are characterized by mountainous relief. By contrast, the Dahomey Gap, which includes parts of Ghana, Togo and Benin, with annual rainfall total of 1000 to 1200 mm, is abnormally dry for the region (see Fig. 3).

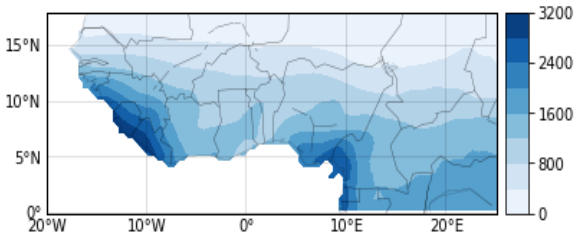

Fig. 3 Average annual rainfall over the period 1901-2016 (mm)

During the twentieth century, the region has experienced several periods of intense drought (UNCCD, WMO and FAO 2018). Widespread and severe droughts have been recorded in the 1910s and 1940s in the Sahelian part. The more severe droughts ravaged the region from 1968 to 1974 and during the early- and mid-1980s. These droughts have caused famines, massive displacements and considerable human loss. The tropical part of West Africa was also affected by these two major droughts but in a more heterogeneous way. More recently, in years 2010-2011, a new drought wave affected the whole region but with a very variable intensity from the Sahelian band to the northern coast of the Gulf of Guinea.

The rainfall data comes from the Climatic Research Unit at the University of East Anglia. We use the gridded time-series of monthly rainfall total at $0.5° \times 0.5°$ latitude/longitude resolution, for the period January 1901 – December 2016. The data was extracted from the revised version of January 2016 of the dataset referred to as CRU TS3.10. The construction of the CRU dataset is detailed in Harris et al (2014). Before proceeding to the estimations, the database had to be cleaned. Prior to 1930, numerous outliers have been detected, especially for cells located in the northern part of the region corresponding to the Sahara border. Therefore, the area above the latitude 18°N has been excluded from the sample. We also dropped from the dataset all total annual rainfall that repeat during two or more consecutive years.

We computed annual rainfall from monthly data. Annual precipitation total is commonly used to assess meteorological drought. A decline in annual total is also a rough indicator of agricultural drought especially in the Sahelian and tropical part of the region where the rainfall season lasts 2 to 6 months and the annual rainfall total is equivalent to the seasonal cumulated rainfall.

4. Estimation results

The mixture model is estimated cell by cell, for annual rainfall total over the period 1901–2016. As a rule, we present only the estimation results for the left tail of the distribution, corresponding to drought events.

4.1. Goodness of fit

According to the Kolmogorov-Smirnov (KS) goodness of fit test, the estimated mixture model provides a satisfactory representation of the data for the vast majority of cells (Fig.4). The KS test rejects the equality of the empirical and the mixture cumulative distribution function (CDF) in 3.5% of cases only. This good result is confirmed by the chi-square test, which rejects the null hypothesis of no significant difference between the observed and expected value in 1.7% of cases only. Results are not presented, but are available upon request.

We also compared the accuracy of the GNG mixture and the gamma distribution, which is used to compute the SPI, on the basis of the Root Mean Square Error (RMSE). The difference in the RMSE of the GNG and the gamma shows that the GNG mixture model better fits the data in 62.9 % of cases. To formally test whether the prediction errors from the GNG and the Gamma are significantly different, we run the test of Diebold and Mariano (1992) corrected for small sample-bias (Harvey et al. 1998). Using the absolute error loss criterion, the test results provided in Fig. 5, show that GNG mixture has better predictive accuracy than the Gamma in 39.4 % of cases. Conversely, the Gamma distribution has better predictive in 23.2 % of cases only. We can conclude that the accuracy of the GNG model is as high as or higher than that of Gamma in 83% of locations. When using the square error loss criterion, the results of the Diebold and Mariano test are not as good but still favorable the GNG model, which accuracy is as high as or higher than that of Gamma in 77% of locations.

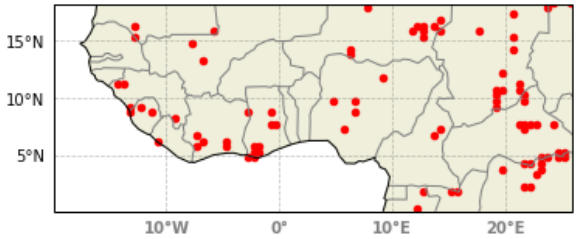

Fig.4 Kolmogorov-Smirnov test. Red cells: bootstrap p-value < 0.05, the GNG does not fit the data.

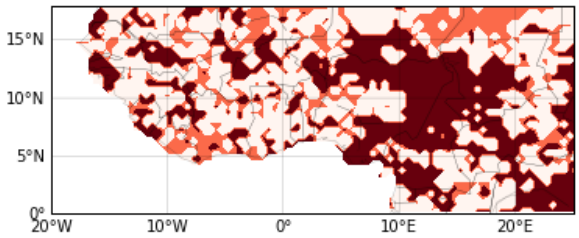

Fig.5 Diebolt and Mariano Test. Loss function: Absolute Error

Brown cells: lower accuracy of the GNG is rejected and higher accuracy of the GNG is not rejected. Orange cells: higher accuracy of the GNG is rejected and lower accuracy of the GNG is not rejected. White cells: the forecasts accuracy of the GNG and of the Gamma are not significantly different.

4.3. Spatial pattern of the GPD parameters

The location parameter of the lower GPD, defining the extreme drought threshold, displays the same latitudinal trend than annual precipitations (Fig. 6 and 7). To allow spatial comparisons, the location parameters are expressed as z-score: $\frac{(x-\mu)}{\sigma}$ with μ and σ the mean

and standard deviation of annual rainfall over the 1981 – 2010 period. Therefore, the standardized values indicate the intensity of the precipitation deficit below which a dry spell can be classified as an extreme drought: the lowest the standardized threshold value, the higher is the intensity of extreme droughts (Fig. 8).

A break appears in the latitudinal organization of the standardized thresholds: they tend to be higher above the 10° latitude and lower below (Fig. 9). Three main clusters of particularly low values appear whose epicenter is located, respectively, in the western part of Nigeria, the southwest and southeast part of the Central African Republic (Fig 8).

The latitudinal trend is less obvious for the scale parameter (σ_l) but there is some evidence of a decreasing trend in sigma above the latitude 12 (Fig. 12 and 13). Below, the spatial distribution of sigma is quite heterogenous. The shape parameter (ξ_l) displays the most erratic spatial pattern (Fig. 14 and 15). In more than 77% of cases, the estimated shape parameter is negative, meaning that the precipitation distribution has a short bounded left tail.

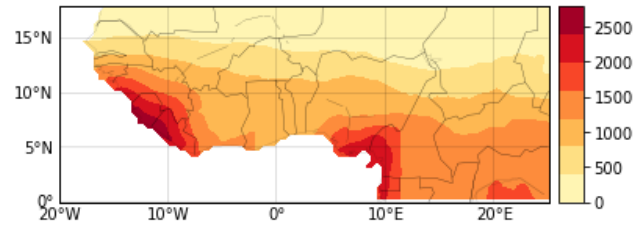

Fig. 6 Extreme drought threshold value in mm (u_l)

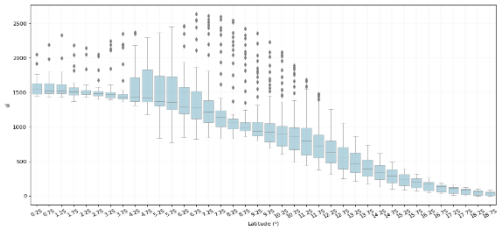

Fig. 7 Extreme drought threshold by latitude

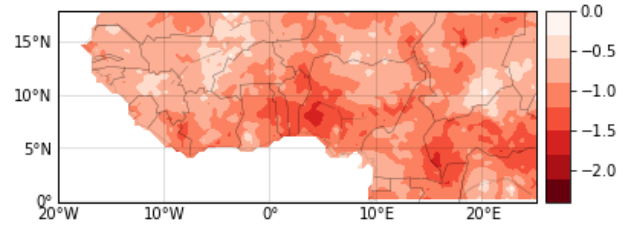

Fig. 8 Standardized drought threshold

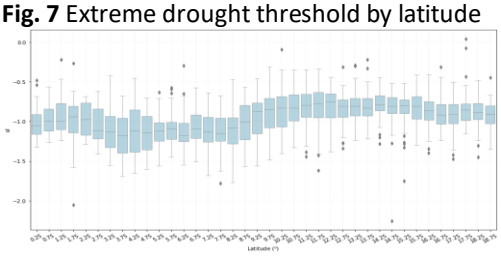

Fig. 9 Standardized drought threshold by latitude

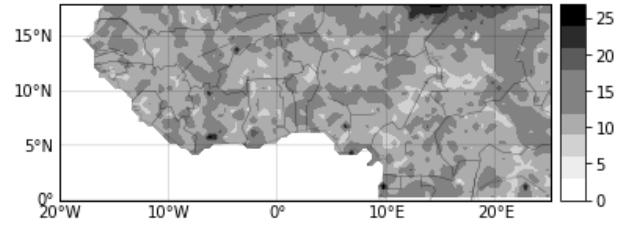

Fig. 10 Probability of being below the left threshold (ϕ_{u_l})

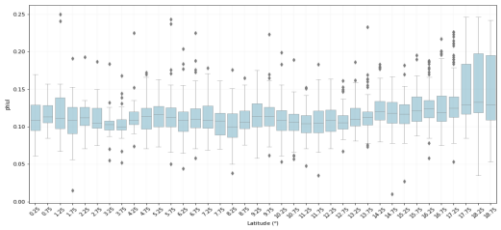

Fig. 11 Probability of being below the left threshold by latitude

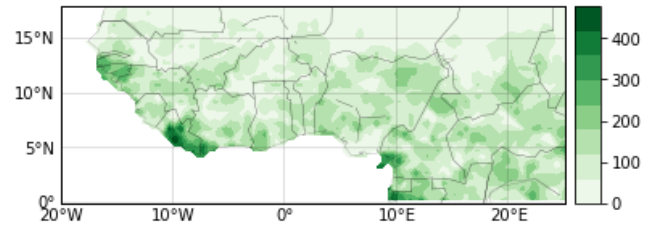

Fig. 12 Scale parameter (σ_l)

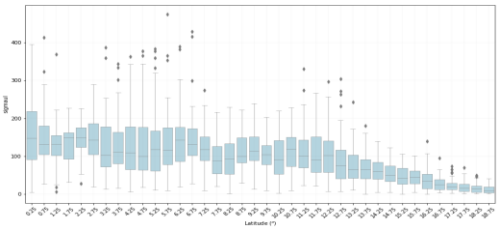

Fig. 13 Scale parameter (σ_l) by latitude

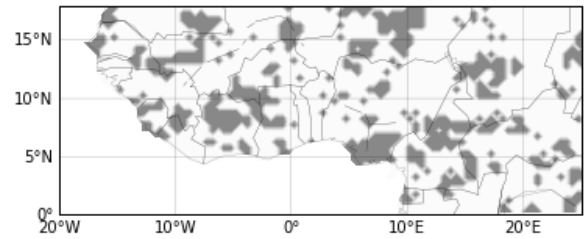

Fig.14 Shape parameter.
$\xi > 0$: Fréchet family; $\xi < 0$ Weibull family

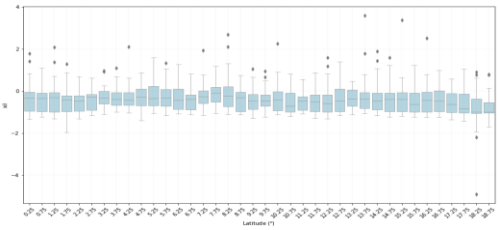

Fig. 15 Shape parameter by latitude

The mixture estimation also gives an implicit parameter, the probability of being below the location parameter or tail fraction (ϕ_u) (Fig. 10). Results show that the probability of non-exceedance the extreme drought threshold is concentrated around its mean (11.4%), with no clear spatial pattern (Fig. 11).

4.4. The Drought hazard and hazard exposure maps

Focusing on extreme droughts we consider that rainfall totals below the extreme value threshold, given by the location parameter of the left GDP, constitute a homogenous category and do not distinguish different classes of droughts below this threshold. Therefore, the drought hazard index (DHI_{gng}) is computed as the product of the minimum intensity of extreme droughts, given by the standardized left threshold value (Z_{ul}), and the probability of being below the threshold (ϕ_{ul}):

$$DHI_{gng} = |Z_{ul}|.\,\phi_{ul} \quad (1)$$

Figure 16 displays the DHI, which has been rescaled using the min-max normalization method. Figure 17 displays the Gi* statistic of Getis and Ord (1992). The G* statistic evidences four clusters of large values of the DHI (hot spots), higher than average. The main one is located in a region covering southwestern Nigeria, southern Benin and Togo. Two other hot spots of drought hazard are located, respectively, in the border area of Cameroon and the Republic of Central Africa (RCA), and in the southeast part of RCA. Last, another spatial area of high values of DHI emerges in the northern edge of the study area, straddling Niger and Chad. By contrast, numerous cold spots, of DHI values lower than average appear. Most of them are located above the 10th parallel.

Figure 18 highlights a U-shape relationship between DHI and latitude: DHI is the lowest between parallel 10 and 15, and higher above and below this band. Clusters of high and low values of DHI alternate from east to west, giving a sinusoidal shape to the relationship between the DHI and the longitude (Fig. 19).

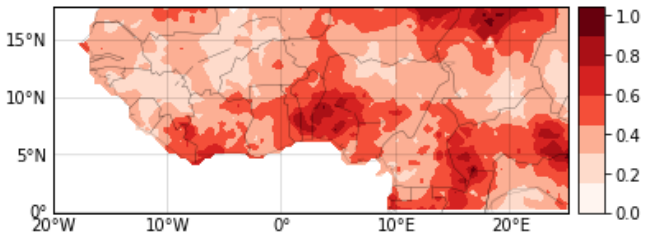

Fig. 16 Rescaled DHI calculated from equation (2).

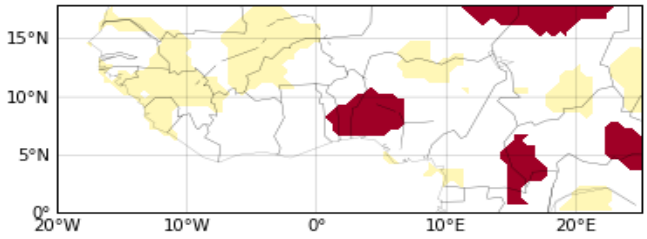

Fig. 17 DHI_1. Getis Ord statistics. Red cells: hot spot (high values) of DHI; yellow cells: cold spot (low values)

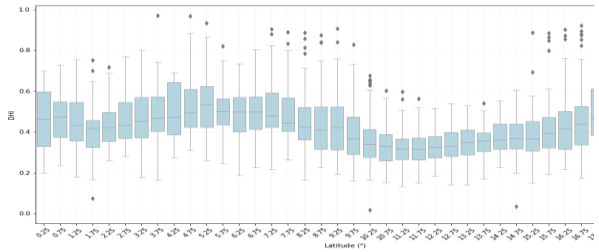

Fig. 18 DHI by latitude

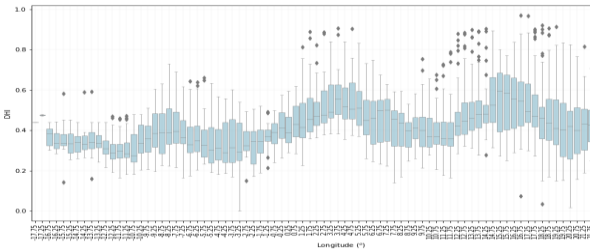

Fig. 19 DHI by longitude

5. Comparison with the standard approach of drought hazard

To assess the relevancy of our approach to drought hazard estimation, we compare our estimation of the DHI with that obtain following the standard approach, and compare the ability of the GNG mixture and the SPI to model extreme droughts.

5.1. The drought hazard index

Drought hazard is commonly defined as a combination of the intensity of droughts and their frequency, and estimated from the SPI and the drought classification of McKee et al (1993) (Table 1). Droughts are classified according to a fixed set of thresholds, and the probability of occurrence of a drought of a given intensity is the same whatever the geographical location and the statistical characteristics of the raw data. Therefore, the intensity of droughts is caught through a fixed weighting, and the DHI is given by:

$$DHI_{spi} = \sum_{i=1}^{4} W_i \times f_i \qquad (2)$$

W_i is the weight assigned to droughts of class i (Table 1, col.2); f_i is the frequency of droughts of type i, namely the number of drought events of type i recorded during the period over the number of observations in the period (table 1, col.5). The DHI_{spi} map is given by Fig. 20.

Drought category	W	Threshold values for the SPI	prob. of occurrence	Empirical frequency: SPI	Thresholds for the GNG in percentiles	prob. of occurrence	Empirical frequency: GNG
Mild drought	0	$]-1\,;\,0]$	34 %	*0.339*	$]16\%\,;\,50\%]$	34%	*0.354*
Moderate drought	1	$]-1.5;\,-1]$	9.2%	*0.083*	$]7\%\,;16\%]$	9%	*0.088*
Severe drought	2	$]-2;\,-1.5]$	4.4%	*0.040*	$]\,2\%;\,7\%]$	5%	*0.043*
Extreme drought	3	≤ -2	2.3%	*0.029*	$\leq 2\%$	2%	*0.020*

Table 1. Drought type designation and thresholds. DHI. W: weight

For comparison purposes, we recalculate our DHI measure, based on the GNG mixture, distinguishing four categories of drought intensity with occurrence probabilities closed to that of McKee (Table 1, col. 6 and 7). We measure the intensity of a class of drought by the standardized value of the upper threshold of each class. Thus, the DHI is given by:

$$DHI_{gng} = \sum_{i=1}^{3} |z_i| \times f_i \qquad (3)$$

With z_1: the standardized value of the 16th percentile; z_2: the standardized value of the 7th percentile; z_3: the standardized value of the 2nd percentile of the GNG distribution. The corresponding map is given by Fig.21.

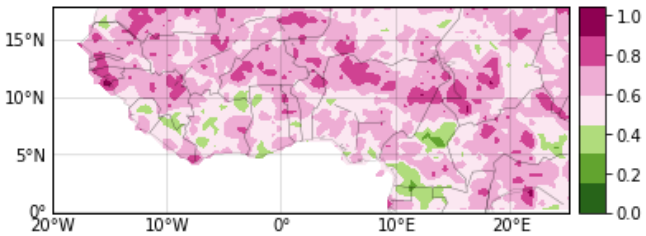

Fig. 20 Rescaled DHI calculated using the SPI and equation (2)

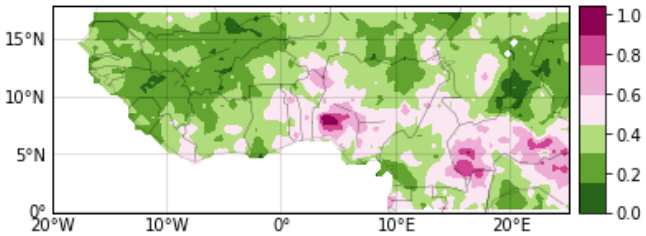

Fig. 21 Rescaled DHI calculated using the GNG model and equation (3)

The two maps, Fig. 20 and Fig. 21 give a very different picture of the spatial distribution of the drought hazard. According to the standard approach (Fig. 20), the draught hazard is higher in the Sahelian band and on the western side of the studied area: Senegal, Guinea Bissau, Guinea, Burkina Faso, Northern Nigeria, and Southern Chad. By contrast, according to our approach, the drought hazard is higher in the southern quadrant of the region (Fig. 21).

These differences are mainly due to the standardization process. In the standard approach, the thresholds, and consequently the intensity of the various drought categories (*W*i), are the same for all series. In our approach, the drought classification is based on percentiles of the theoretical distribution of the raw data. The thresholds and consequently the intensity of the various drought categories, $|z_i|$, vary according to the characteristics of each rainfall distribution.

Another source of divergence, of lesser importance, comes from the unequal quality of adjustment of the data. While the empirical frequency of the different types of droughts (*f*i) should the same in the two approaches, and closed to their theoretical probability of occurrence, some discrepancies appear (Table 1, col 5 and 8). Unsurprisingly, the GNG model performs better to predict extreme drought. This point is explored below.

5.2. Distribution of precipitation in the lower tail

The drought classification in Table 2, col.1, is that commonly used by the US Drought Monitor (USDM) (Sovboda et al 2002). Thresholds are given by percentiles of the rainfall distribution (col. 2). Column.3 gives the corresponding SPI values *i.e*. the percentiles of the Gaussian law. Column 4 gives the theoretical probability of occurrence of each type of drought while columns 5 and 6 give the mean frequency of each drought type using alternatively the SPI values or the GNG percentiles as thresholds.

Drought categories (USDM)	Percentiles	SPI values	Theoretical prob. of occurrence	Empirical frequency: SPI	Empirical frequency: GNG
Abnormally dry	]20% ; 30%]	] –0.84; –0.53]	10%	0.093	0.105
Moderate drought	]10% ; 20%]	] –1.29; –0.84]	10%	0.091	0.098
Severe drought	]5% ; 10%]	] –1.65; –1.29]	5%	0.044	0.044
Extreme drought	]2% ; 5%]	] –2.05; –1.65]	3%	0.027	0.025
Exceptional drought	≤2%	≤–2.05	2%	0.026	0.020
Total			30%	0.281	0.292

Table 2. Probability of occurrence and empirical frequency of drought categories. Empirical frequency is the mean frequency over the whole sample, which includes 2981 locations and 263754 annual rainfall observations.

We can see that the GNG mixture performs better than the SPI to model the left tail of the rainfall distribution, with 29.2% of observations below the 30th percentile compared to 28.1% for the SPI. When looking at the distribution of observations below the 30th percentile, the GNG is better at modeling the highest and lowest percentiles corresponding, on the one hand, to the “abnormally dry” and “moderate drought” categories and, on the other hand, to “exceptional drought”. Both the SPI and the GNG perform poorly in detecting “severe droughts” between the 10th and 5th percentiles.

5.3. The centennial drought

The centennial drought has a return period of 100 years and a return level equals to the first percentile of the distribution. Therefore, the 100 years return level is the amount of annual rainfall total that can be expected on average in 1 year out of 100 years. Considering these

centennial droughts, the GNG mixture model appears more efficient than the standard approach based on the SPI to model these events.

The number of dry spells with an annual rainfall total less than or equal to that of the 100-year drought, differs greatly depending on whether it is calculated using the GNG or the SPI distribution (Table 3). According to the SPI approach, almost 12% of locations did not experience a rainfall episode equal to or below the 100-year drought level while 19% of locations experienced more than 2 drought years below the 100-years level, in the period 1901 - 2016. Results are more consistent when using the GNG distribution: less than 1% of locations did not experienced a drought spell below the 100-years drought level, and only 2.7% of locations experienced more than 2 drought episodes below the 100-years level.

	SPI		GNG	
Value	Count	Percent	Count	Percent
0	278	11.59	19	0.79
1	881	36.72	1554	64.78
2	785	32.72	760	31.68
3	352	14.67	60	2.50
4	92	3.83	5	0.21
5	11	0.46	1	0.04
Total	2399	100.00	2399	100.00

Table 3. Frequency of 100-years drought episodes in the period 1901 - 2016

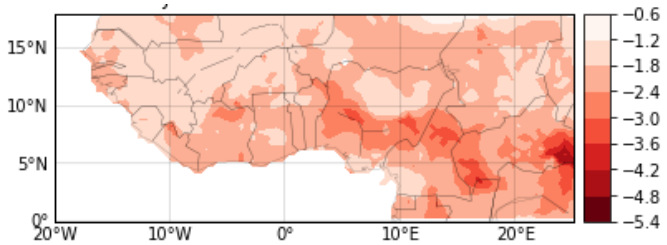

Fig. 22 GNG 100-year drought level: standardized values

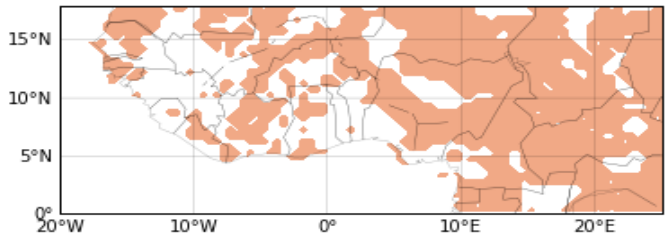

Fig. 23 Brown cells: the intensity of the centennial drought predicted by the GNG is higher than that predicted by the Gamma

Figure 22 shows the intensity of the centennial drought calculated from the GNG distribution, and measured by the standardized return value. The comparison with the intensity of the centennial drought calculated from the gamma distribution, shows that in a majority of cases (63.4%), the Gamma minimizes the severity of the centennial drought (Fig. 23). In other words, if the GNG is a good approximation of the rainfall distribution, using the Gamma, will lead to underestimate the severity of the centennial drought.

6. Conclusion

To design efficient drought risk management and risk coping strategies, at the national or regional level, we need above all information on the temporal and spatial distribution of precipitation. This information is necessary to assess drought hazard and hazard prone locations. A critical stage in drought hazard assessment is the definition of a drought event, and the classification of droughts. While the standard method is based on an *ad hoc* fixed set of thresholds, the method we propose aims at providing an objective definition and a measure of drought, based on the statistical properties of the rainfall distribution.

We consider the class of droughts that are potentially damaging, which distribution can be approximated by an extreme value model. The extreme drought threshold is not set exogenously but estimated using the mixture model with a generalized Pareto distribution for the upper and lower tails, and a normal for the center of the distribution. The extreme drought threshold is given by the location parameter of the lower tail GPD and the probability of precipitation below the threshold is given by the lower tail fraction. Therefore, the two components of drought hazard, the drought threshold and the drought probability, are idiosyncratic, dependent on the specific characteristics of precipitation data.

Another advantage of the proposed method is its operational aspect. The drought threshold can be easily estimated and the estimation accuracy tested. The drought threshold is measured in the same unit than the rainfall data, in mm per year in our case, so that a rainfall deficit can be readily classified and appropriate responses quickly triggered.

The application conducted on the West Africa region and an indicator of meteorological drought, shows the great sensitivity of results to the method used to estimate the drought hazard. The use of the SPI to identify extreme drought leads to underestimate the intensity of extreme droughts, and to an abnormally high frequency of extreme events with a return period of 100 years or more. This result potentially challenges many research studies that use the SPI to identify rainfall shocks and estimate their economic and social impact.

Last the map of drought hazard index offer a different picture of the spatial distribution of the hazard prone locations. Our drought hazard measure shows more heterogeneity across locations than the standard one. More important, our results show that the climatic regions more favorable to agricultural production are also the more exposed to extreme droughts. Considering that the annual rainfall is a rough indicator for agricultural drought, the results should lead to pay a greater attention to the wetlands, which are the most agriculture intensive and where the intensity of extreme droughts is the highest.

This analysis should be considered as exploratory. Its scope could be extended to a larger geographic area, and to other indicators of drought. In drought hazard assessment, the assumptions made on the rainfall distribution are crucial and the relevancy of the drought hazard estimates depends on the goodness of fit of the assumed distribution. The tests and the distribution of drought events show that the mixture model better fit the data than the standardization process used to calculate the SPI. However, a still better fitting model can be looked for in further research.

8. References

Carrão H, Naumann G & Barbosa P (2016) Mapping Global Patterns of Drought Risk: An Empirical Framework Based on Sub-National Estimates of Hazard, Exposure and Vulnerability. *Global Environmental Change* 39 (July): 108–24. https://doi.org/10.1016/j.gloenvcha.2016.04.012.

Carrão H, Singleton A, Naumann G, Barbosa P & Vogt JV (2014) An Optimized System for the Classification of Meteorological Drought Intensity with Applications in Drought Frequency Analysis. *Journal of Applied Meteorology and Climatology* 53 (8): 1943–60. https://doi.org/10.1175/JAMC-D-13-0167.1.

Diebold FX & Mariano R (2002) Comparing Predictive Accuracy. *Journal of Business & Economic Statistics* 20 (1): 134–44. https://doi.org/10.1198/073500102753410444.

Dilley M, Chen RS, Deichmann U, Lerner-Lam AL, Arnold M (2005) Natural Disaster Hotspots: A Global Risk Analysis. Washington, DC: World Bank. © World Bank. https://openknowledge.worldbank.org/handle/10986/7376 License: CC BY 3.0 IGO.

Edwards D & McKee T (1997) Characteristics of 20th century drought in the United States at multiple time scales. *Climatology Report 97-2*, Department of Atmospheric Science, Colorado State University, Fort Collins, Colorado.

Guttman NB (1999) Accepting the Standardized Precipitation Index: A Calculation Algorithm[1]. *JAWRA Journal of the American Water Resources Association* 35 (2): 311–22. https://doi.org/10.1111/j.1752-1688.1999.tb03592.x.

Harvey D, Leybourne SJ & Newbold N (1998) Tests for Forecast Encompassing. *Journal of Business & Economic Statistics*, 16:2, 254-259, DOI: 10.1080/07350015.1998.10524759

Getis A & Ord JK (1992) The Analysis of Spatial Association by Use of Distance Statistics. *Geographical Analysis*, 24 (3): 189-206.

Harris I, Jones PD, Osborn TJ & Lister DH (2014) Updated high-resolution grids of monthly climatic observations – the CRU TS3.10 Dataset. *International Journal of Climatology*, 34: 623–642. doi: 10.1002/joc.3711

Hayes MJ, Wilhelmi OV & Knutson CL (2004) Reducing Drought Risk: Bridging Theory and Practice. *Natural Hazards Review* 5 (2): 106–13. https://doi.org/10.1061/(ASCE)1527-6988(2004)5:2(106).

He B, Wu J, Lü A, Cui X, Zhou L, Liu M, & Zhao L (2013) Quantitative Assessment and Spatial Characteristic Analysis of Agricultural Drought Risk in China. *Natural Hazards* 66 (2): 155–66. https://doi.org/10.1007/s11069-012-0398-8.

Hu Y & Scarrott C (2018) *evmix: Extreme Value Mixture Modelling, Threshold Estimation and Boundary Corrected Kernel Density Estimation*. R package version 2.10, URL https://CRAN.R-project.org/package=evmix.

IPCC (2012) Managing the Risks of Extreme Events and Disasters to Advance Climate Change Adaptation. A Special Report of Working Groups I and II of the Intergovernmental Panel on Climate Change [Field, C.B., V. Barros, T.F. Stocker, D. Qin, D.J. Dokken, K.L. Ebi, M.D. Mastrandrea, K.J. Mach, G.-K. Plattner, S.K. Allen, M. Tignor, and P.M. Midgley (eds.)]. Cambridge University Press, Cambridge, UK, and New York, NY, USA, 582 pp. https://www.ipcc.ch/site/assets/uploads/2018/03/SREX_Full_Report-1.pdf

McKee T, Doesken NJ & Kleist J (1993) The relationship of drought frequency and duration to time scales, Eighth Conference on Applied Climatology, Anaheim, California.

Ó Gráda C (2007) Making Famine History. *Journal of Economic Literature* 45 (1): 5–38. https://doi.org/10.1257/jel.45.1.5.

Palmer WC (1965) Meteorological Drought. *Research Paper* No. 45, US Weather Bureau, Washington, DC. https://www.ncdc.noaa.gov/temp-and-precip/drought/docs/palmer.pdf.

Rajsekhar D, Singh VP, and Mishra AK (2015) Integrated Drought Causality, Hazard, and Vulnerability Assessment for Future Socioeconomic Scenarios: An Information Theory Perspective. *Journal of Geophysical Research: Atmospheres* 120 (13): 6346–78. https://doi.org/10.1002/2014JD022670.

Scarrott C & MacDonald A (2012) A review of extreme value threshold estimation and uncertainty quantification. REVSTAT - Statistical Journal 10(1), 33-59

Shahid S, and Behrawan H (2008) Drought Risk Assessment in the Western Part of Bangladesh. *Natural Hazards* 46 (3): 391–413. https://doi.org/10.1007/s11069-007-9191-5.

Svoboda MD & Coauthors (2002) The drought monitor. Bulletin of the American Meteorological Society, 83(8), 1181–1190.

UNCCD, WMO & FAO (2018) *Strategic framework for drought risk management and enhancing resilience in Africa*, White Paper, Bonn, Germany.

Vicente-Serrano SM, Beguería S, López-Moreno JI (2010) A Multiscalar Drought Index Sensitive to Global Warming: The Standardized Precipitation Evapotranspiration Index. *Journal of Climate* 23 (7): 1696–1718. https://doi.org/10.1175/2009JCLI2909.1.

Wilhite DA (2000) Drought as a natural hazard: concepts and definitions. in D. A. Wilhite (Ed) *Drought: A Global Assessment*, Vol. I, chap. 1, Routledge Publishers, UK, pp. 3–18.

Wilhite DA & Glantz MH (1985) Understanding: The Drought Phenomenon: The Role of Definitions. *Water International* 10 (3): 111–20. https://doi.org/10.1080/02508068508686328.

Wilhite DA, Sivakumar MVK & Pulwarty R (2014) Managing Drought Risk in a Changing Climate: The Role of National Drought Policy. *Weather and Climate Extremes* 3 (June): 4–13. https://doi.org/10.1016/j.wace.2014.01.002.

Wilhite DA, Svoboda MD & Hayes MJ (2007) Understanding the Complex Impacts of Drought: A Key to Enhancing Drought Mitigation and Preparedness. *Water Resources Management* 21 (5): 763–74. https://doi.org/10.1007/s11269-006-9076-5.

WMO (2012) *Standardized Precipitation Index User Guide*, WMO-No. 1090, Geneva.

WMO & GWP (2016) *Handbook of Drought Indicators and Indices* (M. Svoboda and B.A. Fuchs). Integrated Drought Management Programme (IDMP), Integrated Drought Management Tools and Guidelines Series 2. Geneva.